This is an open access article published under a Creative Commons Attribution (CC-BY) License, which permits unrestricted use, distribution and reproduction in any medium, provided the author and source are cited.

ACS AUTHORCHOICE

JACS
JOURNAL OF THE AMERICAN CHEMICAL SOCIETY

pubs.acs.org/JACS

Article

# Transmembrane Ion Channels Formed by a Star of David [2]Catenane and a Molecular Pentafoil Knot

David P. August, Stefan Borsley, Scott L. Cockroft, Flavio della Sala, David A. Leigh,* and Simon J. Webb

Cite This: *J. Am. Chem. Soc.* 2020, 142, 18859–18865

Read Online

ACCESS | Metrics & More | Article Recommendations | Supporting Information

**ABSTRACT:** A $(Fe^{II})_6$-coordinated triply interlocked ("Star of David") [2]catenane ($6_1^2$ link) and a $(Fe^{II})_5$-coordinated pentafoil ($5_1$) knot are found to selectively transport anions across phospholipid bilayers. Allostery, topology, and building block stoichiometry all play important roles in the efficacy of the ionophoric activity. Multiple $Fe^{II}$ cation coordination by the interlocked molecules is crucial: the demetalated catenane exhibits no anion binding in solution nor any transmembrane ion transport properties. However, the topologically trivial, Lehn-type cyclic hexameric $Fe^{II}$ helicates—which have similar anion binding affinities to the metalated Star of David catenane in solution—also display no ion transport properties. The unanticipated difference in behavior between the open- and closed-loop structures may arise from conformational restrictions in the linking groups that likely enhances the rigidity of the channel-forming topologically complex molecules. The $(Fe^{II})_6$-coordinated Star of David catenane, derived from a hexameric cyclic helicate, is 2 orders of magnitude more potent in terms of ion transport than the $(Fe^{II})_5$-coordinated pentafoil knot, derived from a cyclic pentamer of the same building block. The reduced efficacy is reminiscent of multisubunit protein ion channels assembled with incorrect monomer stoichiometries.

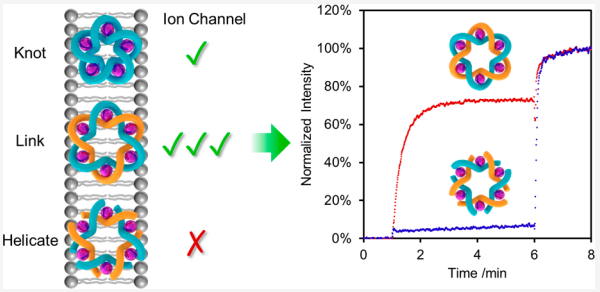


## INTRODUCTION

The orderly entanglement of molecular strands within knots[1] and links[2] (catenanes) can induce properties and characteristics[1a2a] that are beginning to be explored in areas as diverse as anion binding,[3] catalysis,[4] materials,[5] health care,[6] and the kinetic stabilization of supramolecular structures.[7] One strategy to synthesize examples of complex molecular topologies is to join the ends of building blocks that assemble into cyclic metal double helicates.[1a,8,9] In a typical example, by tuning of the assembly conditions, the same set of components can be enticed to selectively form either a five-membered or a six-membered Lehn-type cyclic helicate.[8] Subsequent macrocyclization of the building block end groups by ring-closing metathesis gives the corresponding pentafoil ($5_1$) knot[4a] or Star of David triply interlocked [2]catenane ($6_1^2$ link),[9c] respectively (Scheme 1). The metalated knot, link, and the parent open cyclic helicates display good to very strong halide binding affinities in their central cavities ($K_a \approx 10^5$–$10^{10}$ $M^{-1}$ in MeCN).[3a] The anion-binding properties of the interiors of these metal-coordinated molecular structures led us to investigate their potential as transmembrane ion channels or transporters.[10]

Protein ion channels typically have complex secondary, tertiary, and quaternary structures that determine their transport properties.[11] For example, membrane-spanning proteins often consist of $\alpha$-helix bundles or $\beta$-barrels, which confer rigidity and anchor the protein within the membrane. In contrast, small-molecule systems are generally much less complex[12] and rely on intermolecular interactions, such as hydrogen bonding[13] and aromatic stacking,[13f,14] to promote their assembly into rigid membrane-spanning ion channels. Metal ion-ligand coordination can also be used to assemble ionophoric supramolecular structures, and a number of metallo-organic ion transporters have also been described.[15] We reasoned that the high anion affinities[3a] and the rigid shape with internal cavity imposed by the topology of the metalated pentafoil knot **2**[4a] and Star of David link **3**[9c] could make them suitable candidates for ion transportation (Scheme 1). Furthermore, the two molecular structures are assembled from the same repeat unit, **1**, allowing the direct comparison of assemblies of the same building block in two different stoichiometries.

A series of assays in phospholipid vesicles were used to examine the ion transport behavior and selectivity of **2** and **3** (Figure 1). The metalated pentafoil knot was used as the monochloride salt (other anions $PF_6^-$), **2**, because the fully hexafluorophosphate salt rapidly exchanges one $PF_6^-$ for a $Cl^-$ ion by sequestering traces of chloride from glassware or

**Received:** July 24, 2020
**Published:** October 21, 2020


© 2020 American Chemical Society

https://dx.doi.org/10.1021/jacs.0c07977
*J. Am. Chem. Soc.* 2020, 142, 18859–18865

**Scheme 1. Synthesis of $(Fe^{II})_5$-Coordinated Pentafoil Knot Complex 2 and $(Fe^{II})_6$-Coordinated Star of David [2]Catenane Complex 3 from Ligand 1**[a]

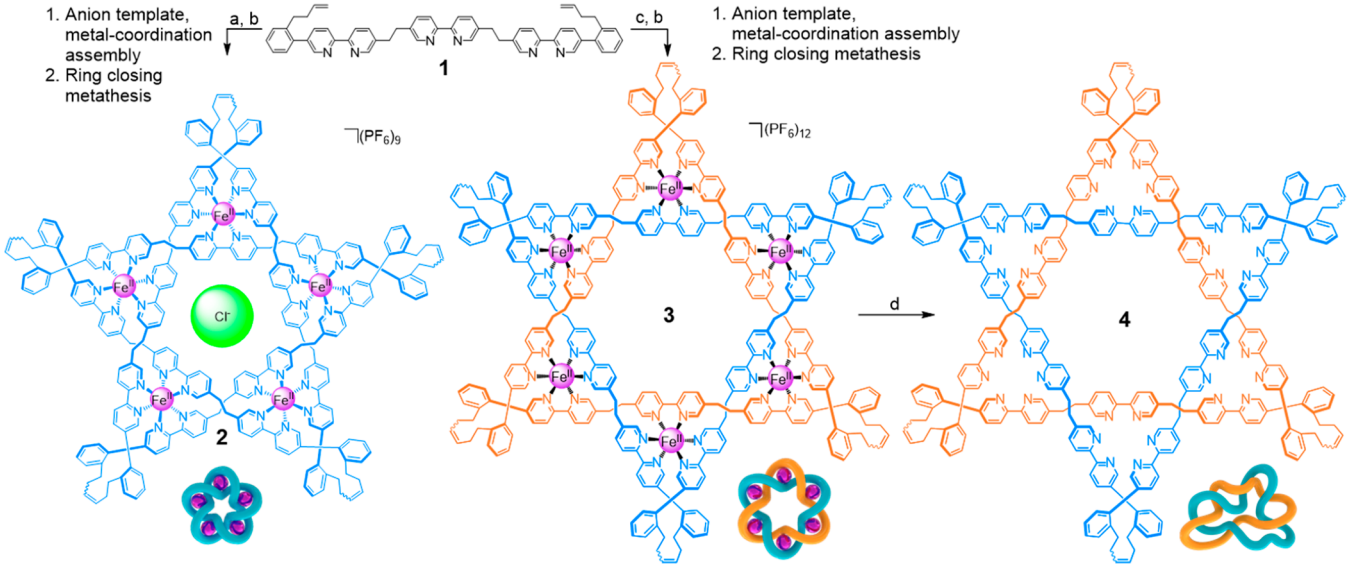


[a]Pentafoil knot **2** is isolated and used with a chloride anion bound in the central cavity. The Star of David [2]catenane **3** was treated with $Na_4EDTA$ to generate the demetalated link **4**. [b]Reagents and conditions: (a) $FeCl_2$, dimethyl sulfoxide, 60 °C, 24 h followed by excess saturated aqueous $KPF_6$ solution; (b) Hoveyda-Grubbs second-generation catalyst $(H_2IMes)Cl_2RuCH(o\text{-}O^iPrC_6H_4)$, 1,2-dichloroethane/$MeNO_2$ (1:1), 60 °C, 24 h followed by excess saturated aqueous $KPF_6$ solution; (c) $FeSO_4{\cdot}7H_2O$, ethylene glycol, 170 °C, 24 h followed by excess saturated $KPF_6$ in methanol; (d) $Na_4EDTA$ (EDTA = ethylenediaminetetraacetic acid), $H_2O$/MeCN (1:1), 80 °C, 4 h.

solvent.[3a] The somewhat less halophilic metalated Star of David catenane was used as the fully hexafluorophosphate salt, **3**. The ion transport abilities of the metalated knot and link were compared with that of the demetalated Star of David catenane, **4**, which without transition-metal coordination exhibits no anion binding in solution, and $Fe^{II}$-coordinated Lehn-type open cyclic hexameric helicates (**5** and **6**), to determine the influence of (i) metal-binding allostery and (ii) molecular topology (Figure 2). The results of the vesicle experiments were corroborated by single-channel planar bilayer conductance measurements (Figure 3).

## EXPERIMENTAL DETAILS

The $Fe^{II}$-coordinated pentafoil knot **2**[4a] and the Star of David [2]catenane **3**[9c] were prepared from ligand **1** in the presence of different $Fe^{II}$ salts followed by ring-closing olefin metathesis (Scheme 1). The ionophoric activity of the compounds in the vesicles was initially assessed in 8-hydroxypyrene-1,3,6-trisulfonate (HPTS) assays using 4:1 v/v egg yolk phosphatidylcholine (EYPC)/cholesterol vesicles in 3-(*N*-morpholino)propanesulfonic acid (MOPS) buffer (15.2 mM lipid, [MOPS] = 20 mM, pH 7.4).[16] In these experiments, vesicles containing HPTS and different salts were prepared ([salt] = 100 mM, see Section S3.1, Supporting Information). Either knot **2** or link **3** (2.5 $\mu$M, 0.26 mol % relative to EYPC/cholesterol) was added to the solution containing the vesicles, followed by a pulse of NaOH (6.5 $\mu$M). Ionophoric activity was indicated by dissipation of the resultant pH gradient between the interior and exterior of the vesicles, which was monitored through the change in the relative fluorescence of HPTS (Figure 1A). Finally, the vesicles were lysed by the addition of a detergent (Triton X-100) to allow normalization of the fluorescence response. The resulting kinetic data were fitted to pseudo-first-order rate equations as an approximation[13f,17] to compare the effectiveness of the analyzed compounds (see Tables S1–S3). Background rates for ion leakage across the membranes for a range of salts were measured (see Figures S6 and S7) and the values subtracted from the knot/link-mediated ion transport rates.

## RESULTS AND DISCUSSION

We first examined the ionophoric activity of the knot and link with respect to KBr (Figure 1B). The $(Fe^{II})_5$-coordinated pentafoil knot **2** displayed weak ion transport activity ($k_{obs}$ = $4.05 \times 10^{-4}$ $s^{-1}$, see Figure S9), while $(Fe^{II})_6$-coordinated Star of David catenane **3** was >50-fold more active ($k_{obs}$ = $2.30 \times 10^{-2}$ $s^{-1}$, see Figure S8). The pentafoil knot and Star of David link both showed significant ion transport and differ only in the number of units of **1** included in their assembly (five and six, respectively). This difference alters both the size of the central hole and the number of cations associated with each structure. It is somewhat reminiscent of the outcome of subunit assembly with the wrong stoichiometry in some biological channels and pores; misassembly with respect to the number of building blocks still results in a functional ion channel but with greatly reduced efficacy of transport.[18]

The $Fe^{II}$-coordinated knot and link are significantly different from the metal-free Star of David catenane ligand **4** in that the bound metal ions confer structural rigidity, add multiple positive charges, and inductively withdraw electron density from the pyridine rings, all of which create the strong anion binding site in the central cavity (Figures S1 and S3). As expected from its lack of anion binding affinity in solution, the demetalated Star of David link **4** showed no activity in the HPTS assay. Allostery, in the form of the coordination of $Fe^{II}$ cations, is an essential feature to enable both anion binding in solution and anion transmembrane transport by **2** and **3**. Nonetheless, the charge provided by complexation to $Fe^{II}$ is not in itself sufficient to cause ion transport; simple $Fe^{II}(bipy)_3$ complexes, such as $FeCl_2(bipy)_3$, showed no ion transport in analogous experiments (Figure S12).

To determine the significance of the interlocked molecular topology in the ion transport experiments, we also tested two Lehn-type circular metal helicates: methyl-derivative **5** and **6**,


https://dx.doi.org/10.1021/jacs.0c07977
J. Am. Chem. Soc. 2020, 142, 18859−18865

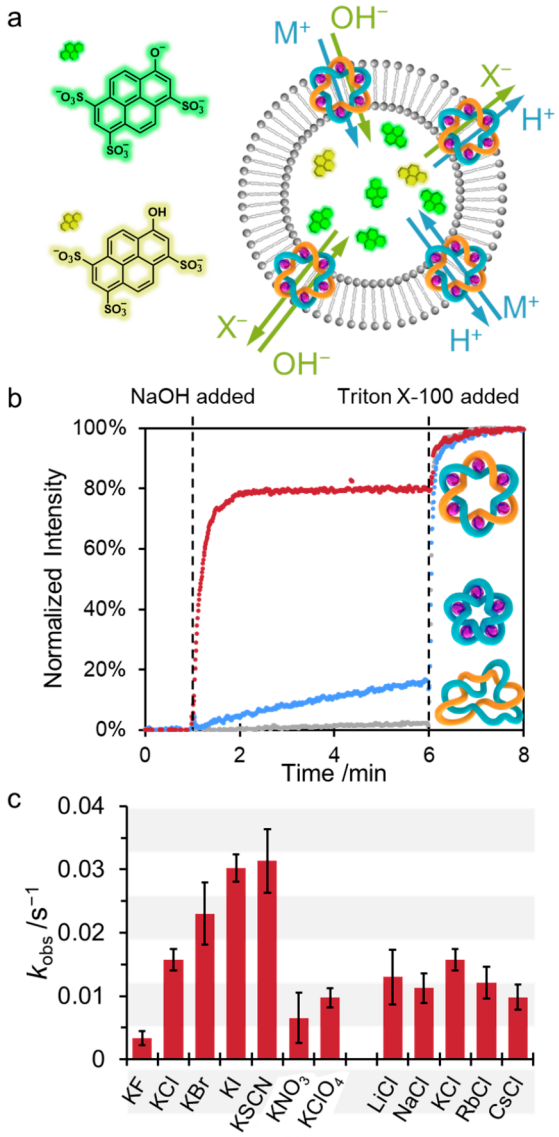


**Figure 1.** (a) Schematic representation of the 8-hydroxypyrene-1,3,6-trisulfonate (HPTS) assay used to determine the ionophoric activity of **2** and **3** in vesicles; internal pH change can occur through any combination of antiport ($M^+/H^+$, $A^-/OH^-$) or symport ($M^+/OH^-$, $A^-/H^+$), as shown.[13] (b) Normalized fluorescence data for HPTS assays with EYPC/cholesterol vesicles formed in the presence of KBr, following the addition of $(Fe^{II})_5$-coordinated pentafoil knot **2** (blue), $(Fe^{II})_6$-coordinated Star of David link **3** (red), or demetalated Star of David link **4** (gray). NaOH base pulse (13 $\mu$L, 1 M) at 1 min, Triton X-100 (20 $\mu$L, 10% v/v solution) at 6 min (EYPC/cholesterol 4:1 v/v vesicles, [compound] = 2.5 $\mu$M, 100 mM KBr 20 mM 3-(*N*-morpholino)propanesulfonic acid (MOPS), pH 7.4). (c) Observed pseudo-first-order rate constants determined from HPTS assays for the transport of different salts ([**3**] = 2.5 $\mu$M, 100 mM MX (M = $Li^+$, $Na^+$, $K^+$, $Rb^+$, $Cs^+$, X = $F^-$, $Cl^-$, $Br^-$, $I^-$, $SCN^-$, $NO_3^-$, $ClO_4^-$), 20 mM MOPS, pH 7.4). The background rate was high for the small, basic $F^-$ anion; nonetheless, it showed a low transport rate (<0.005 $s^{-1}$) when this background rate was accounted for.

the immediate precursor to **3** (Figure 2). These metal-coordinated complexes have anion affinities in solution that are very similar to the $(Fe^{II})_6$-coordinated Star of David link **3**.[3a,8] Remarkably, given the activity of the topologically complex compounds **2** and **3**, neither **5** nor **6** showed any activity in HPTS assays with a range of salts (for HPTS assays with **5**, see

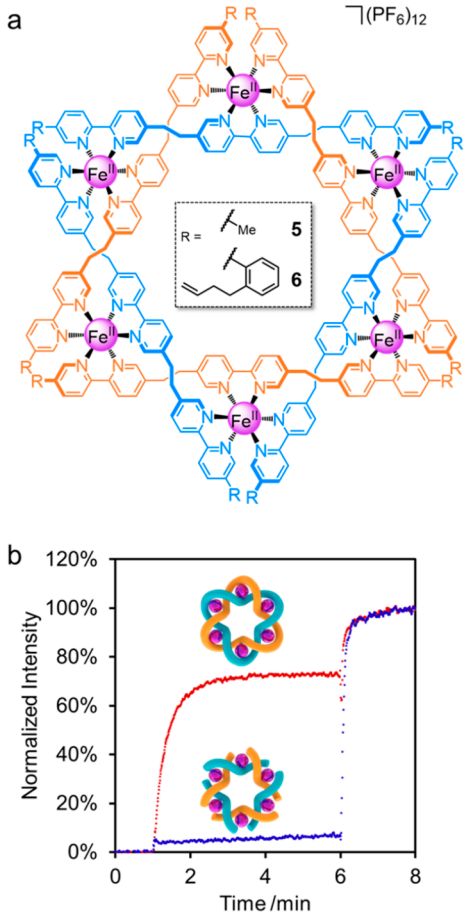


**Figure 2.** (a) Structure of Lehn-type hexameric cyclic helicates **5** and **6**. (b) Representative HPTS assay with $(Fe^{II})_6$-coordinated Star of David catenane **3** and hexameric cyclic helicate **6** ([compound] = 2.5 $\mu$M, 100 mM NaCl, 20 mM MOPS, pH 7.4). NaOH base pulse (13 $\mu$L, 1 M) at 1 min, Triton X-100 (20 $\mu$L, 10% v/v solution) at 6 min.

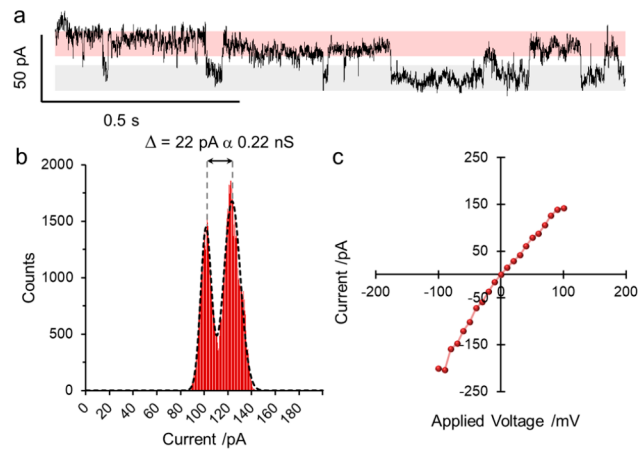


**Figure 3.** Single-channel planar bilayer measurements of ion channel formation by $(Fe^{II})_6$-coordinated Star of David catenane **3** (EYPC lipid/cholesterol (4:1, w/w), [**3**] = 8 $\mu$M, 1 M KCl, 20 mM MOPS, pH 7.4, 293 K). (a) Single-channel recording at +100 mV showing the opening (red) and closing (gray) of a single-ion channel. (b) All-points data analysis (see Section 4.3 of the Supporting Information) of the ion currents recorded at +100 mV. The data were fitted to two Gaussian distributions and the difference in ion current was measured. (c) Current−voltage curves showing the average ion current flow from +100 to −100 mV.



https://dx.doi.org/10.1021/jacs.0c07977
J. Am. Chem. Soc. 2020, 142, 18859−18865

Figure S10; for HPTS assays with **6**, see Figure 3B). The inactivity of **6** is particularly unexpected as it differs from the highly active $(Fe^{II})_6$-coordinated Star of David catenane **3** only in that it has not undergone ring-closing olefin metathesis. It appears that the conformational constraints imposed by joining of the strand ends is crucial for the metalated Star of David catenane **3** to be able to form transmembrane ion channels (although the knot is less effective in doing so). The less ordered ligand exterior is apparent in molecular modeling of helicate **6** (Figure S2).

Having established the strong ionophoric activity of the $(Fe^{II})_6$-coordinated Star of David link **3**, we examined its anion selectivity (Figure 1C, Figure S8). The metalated Star of David link **3** elicited ion transport decreasing in the order KSCN ≈ KI > KBr > KCl > $KClO_4$ ≈ $KNO_3$ > KF. The halides and pseudohalides follow the Hofmeister series,[19] suggesting that desolvation[20] may be the rate-limiting factor for ion transport. However, the transport rates of perchlorate and nitrate differ from that expected from their positions in the Hofmeister series (perchlorate sits between iodide and thiocyanate; nitrate sits between bromide and chloride). Haynes et al. observed a similar effect for $Zn_{10}L_{15}$ cages, which was attributed to size/shape exclusion[15c,21] hindering the passage of the larger perchlorate and nitrate anions.[19,22] Changing the cation showed much less variation in transport rates (Figure 1C, Figure S8d, Table S2), demonstrating that the ionophores are selective only between anions.[15a,23] Anion transport was confirmed by high levels of chloride transport in lucigenin assays (see Section S3.2, Supporting Information).

The mechanism of transport was probed to determine whether the $(Fe^{II})_6$-coordinated pentafoil knot **2** and Star of David catenane **3** were merely disrupting the phospholipid bilayer, acting as an ion carrier or forming ion channels. 5(6)-Carboxyfluorescein assays ruled out vesicle lysis or the formation of large, nonspecific channels (see Section S3.3),[24] while U-tube experiments[25] demonstrated that both the metalated knot **2** and link **3** did not act as carriers (see Section S3.4). These observations suggest that the HPTS assay data arise from anion-selective channels formed in vesicle membranes by the metalated knot and link.

We further investigated the ion channel activity of the molecular knot and link by way of single-channel planar bilayer conductance (PBC) experiments (see Section S4 and Figure 3).[26] A planar bilayer was formed between two wells containing buffer (20 mM MOPS, 1 M KCl, pH 7.4) and a potential applied across the membrane. The channel-forming compound was then added to one well (Figure S19), resulting in step changes in the ion current, indicating the formation of ion channels. While we did not observe current steps with the metalated pentafoil knot **2** within the 2 h duration of the measurement, the addition of the metalated Star of David link **3** led to reproducible, quantized, square-topped "flicker" events[26] (Figure 3A, Figures S20 and S21), indicative of short-lived ion channels. Increased channel formation was observed under negative applied potentials compared to when a positive potential was applied (Figure 3B). This is consistent with the positively charged link **3** being driven toward the membrane.[27] The channels have a high conductance around 0.22 nS (measured at +100 mV, Figure 3C), mirroring the high ionophoric activity observed in the HPTS assays (Figure 1). Hille analysis (Section S4.4) of the PBC data allowed the diameter of the channels formed by **3** to be estimated as 5.0–7.2 Å.

A Hill plot analysis[28] of the HPTS assays for KCl transport by $(Fe^{II})_6$-coordinated Star of David catenane **3** (see Figure S11) gave an $EC_{50}$ value of 1.3 μM (17.4 μg $mL^{-1}$) and a channel stoichiometry of 1 (i.e., a channel is made by a single molecule of **3**). While Hill plot analysis has many underlying assumptions,[29] in combination with the observed ion selectivity, it suggests that the formation of single catenane ion channels able to transport anions (e.g., perhaps through a "relay-race" mechanism[30]) is a reasonable explanation for the observed ionophoric activity.

The overall picture that emerges from the experimental studies of the $(Fe^{II})_6$-coordinated Star of David **3** is that the high ionophoric activity arises from membrane insertion to form channels, which are likely to involve a single molecule of **3** (Hill plot analysis, $n$ = 1, Figure S11). Given its size and relatively hydrophobic edges (Figure S3), we speculate that the catenane could embed in the hydrophobic membrane with its faces parallel to either side of the otherwise intact membrane. Although the thickness of the catenane is significantly less than the thickness of the bilayer, the bilayer may thin around the channel former, as observed for the shorter antibiotics in the peptaibol family.[31]

The markedly better ionophoric activity of the Star of David catenane **3** (constructed from six molecules of building block **1**) over pentafoil knot **2** (made from five molecules of **1**) may be a consequence of the weaker binding of anions (such as $Cl^-$, $Br^-$ and $I^-$) in the larger diameter (~0.46 nm) central hole of **3** (Figure 4).[3a] The X-ray crystal structure[4a] of pentafoil knot **2** shows the tightly bound chloride anion is displaced above the central cavity (Figure S1), with the hole diameter at its narrowest being smaller (~0.24 nm) than the ionic diameter of a chloride ion (~0.36 nm),[22] suggesting that the anion might not easily pass through to the other side. This very tightly bound anion may also have a very slow rate of dissociation, effectively blocking the hole. The anion selectivity of the

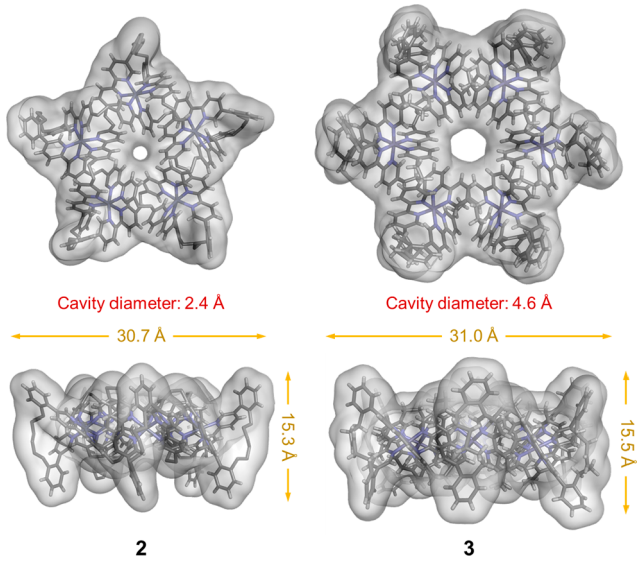


**Figure 4.** Solvent-accessible iso-surface overlaid on X-ray crystal structures of $(Fe^{II})_5$-coordinated pentafoil knot **2** (left)[4a] and $(Fe^{II})_6$-coordinated Star of David link **3** (right)[9c] shown from above (top) and from the side (bottom). The structure dimensions (yellow double-headed arrows) and the diameters of the cavity (red) are shown. A $^1H$ radius of 1 Å, a typical value for hydrogen-bonding H atoms,[20] was assumed for distance measurements (see Section S2.2).



https://dx.doi.org/10.1021/jacs.0c07977
J. Am. Chem. Soc. 2020, 142, 18859–18865

channel formed by **3** broadly follows the relative anion binding affinity of the Star of David catenane in MeCN solution.[3a] The calculated Hille diameter is also similar to the hole diameter in the solid state.[9c] The low rate of perchlorate and nitrate transport relative to their place in the Hofmeister series is also consistent with anion flow through rigid channels of well-defined size and shape, with a partial size-exclusion mechanism being the cause of the observed selectivity.[19,21,22] Nonetheless, we do not rule out an alternative transport mode not involving the central cavity. If the compounds insert perpendicularly into the membrane, the ions may flow around the molecule, as previously observed for certain DNA duplexes,[32] although it is not clear how to rationalize such a mechanism with the observed size/shape departure from the Hofmeister series in anion transport.

## CONCLUSIONS

Our results show that a $(Fe^{II})_6$-coordinated Star of David [2]catenane, **3**, based on a double closed-loop hexameric assembly, exhibits high ionophoric activity in transmembrane ion transport experiments, with anion selectivity governed by anion desolvation energies and size exclusion. The analogous $(Fe^{II})_5$-coordinated pentafoil knot **2**, based on a closed-loop cyclic pentamer of the same building block, also shows ion transport activity but is almost 2 orders of magnitude less active than the Star of David catenane. Allosteric binding of the $Fe^{II}$ ions creates a rigid central anion binding cavity and is crucial for forming ion channels. Remarkably, however, analogous $Fe^{II}$-coordinated Lehn-type cyclic helicates—including the immediate precursor to the Star of David catenane prior to ring-closing metathesis—show no ionophoric activity, despite having similar anion binding affinities to the $Fe^{II}$-coordinated triply interlocked [2]catenane in solution. This dramatic "topology effect" is likely due to conformational restrictions imposed on the chains that link the building blocks in the catenane and knot. Control experiments rule out a carrier mechanism for transport membrane lysis, while single-channel planar bilayer experiments with the $(Fe^{II})_6$-coordinated Star of David catenane, **3**, confirm the formation of ion channels. The level of ion transport activity of the Star of David catenane ($EC_{50}$ for KCl transport = 1.3 $\mu$M, 17.4 $\mu$g $mL^{-1}$) is similar to that of some putative antibiotics.[33] The discovery of a new class of synthetic ion channels for which both allosteric binding and "molecular nanotopology"[34] play vital roles opens up new research directions and the opportunity for creating ion channels that could potentially be tunable or switchable through the use of different metal ions, oxidation states, or coordination geometries.[35]

## ASSOCIATED CONTENT

### Supporting Information

The Supporting Information is available free of charge at https://pubs.acs.org/doi/10.1021/jacs.0c07977.

Experimental section, synthetic overview, fluorescence measurements, UV−vis measurements, planar bilayer measurements, extended data sets, and analysis of previously reported crystal structures (PDF)

## AUTHOR INFORMATION


### Corresponding Author

**David A. Leigh** − *Department of Chemistry, University of Manchester, Manchester M13 9PL, United Kingdom;* orcid.org/0000-0002-1202-4507; Email: david.leigh@manchester.ac.uk

### Authors

**David P. August** − *Department of Chemistry, University of Manchester, Manchester M13 9PL, United Kingdom;* orcid.org/0000-0002-4049-0759

**Stefan Borsley** − *Department of Chemistry, University of Manchester, Manchester M13 9PL, United Kingdom*

**Scott L. Cockroft** − *EaStCHEM School of Chemistry, University of Edinburgh, Edinburgh EH9 3FJ, United Kingdom;* orcid.org/0000-0001-9321-8997

**Flavio della Sala** − *Department of Chemistry and Manchester Institute of Biotechnology, University of Manchester, Manchester M13 9PL, United Kingdom*

**Simon J. Webb** − *Department of Chemistry and Manchester Institute of Biotechnology, University of Manchester, Manchester M13 9PL, United Kingdom;* orcid.org/0000-0001-9793-8748

Complete contact information is available at: https://pubs.acs.org/10.1021/jacs.0c07977


### Notes

The authors declare no competing financial interest.

## ACKNOWLEDGMENTS

We thank the Engineering and Physical Sciences Research Council (EPSRC; EP/P027067/1), the European Research Council (ERC Advanced Grant 786630), and the Leverhulme Trust (Philip Leverhulme Prize for S.L.C.) for funding, and the University of Manchester Mass Spectrometry Service Centre for high-resolution mass spectrometry. D.A.L. is a Royal Society Research Professor.

## REFERENCES

(1) (a) Fielden, S. D. P.; Leigh, D. A.; Woltering, S. L. Molecular knots. *Angew. Chem., Int. Ed.* **2017**, *56*, 11166−11194. (b) Fenlon, E. E. Open Problems in Chemical Topology. *Eur. J. Org. Chem.* **2008**, *2008*, 5023−5035. (c) Forgan, R. S.; Sauvage, J.-P.; Stoddart, J. F. Chemical topology: Complex molecular knots, links, and entanglements. *Chem. Rev.* **2011**, *111*, 5434−5464. (d) Ayme, J.-F.; Beves, J. E.; Campbell, C. J.; Leigh, D. A. Template synthesis of molecular knots. *Chem. Soc. Rev.* **2013**, *42*, 1700−1712. (e) Horner, K. E.; Miller, M. A.; Steed, J. W.; Sutcliffe, P. M. Knot theory in modern chemistry. *Chem. Soc. Rev.* **2016**, *45*, 6432−6448. (f) Sauvage, J.-P. From chemical topology to molecular machines (Nobel Lecture). *Angew. Chem., Int. Ed.* **2017**, *56*, 11080−11093. (g) Lim, N. C. H.; Jackson, S. E. Molecular knots in biology and chemistry. *J. Phys.: Condens. Matter* **2015**, *27*, 354101. (h) Cougnon, F. B. L.; Caprice, K.; Pupier, M.; Bauza, A.; Frontera, A. A strategy to synthesize molecular knots and links using the hydrophobic effect. *J. Am. Chem. Soc.* **2018**, *140*, 12442−12450. (i) Guo, B.-B.; Lin, Y.-J.; Jin, G.-X. Design and stability studies of trefoil knots featuring RhCp* building blocks. *Chem. - Eur. J.* **2019**, *25*, 9721−9727.

(2) (a) Gil-Ramírez, G.; Leigh, D. A.; Stephens, A. J. Catenanes: Fifty years of molecular links. *Angew. Chem., Int. Ed.* **2015**, *54*, 6110−6150. (b) Au-Yeung, H. Y.; Yee, C.-C.; Ng, A. W. H.; Hu, K. Strategies to assemble catenanes with multiple interlocked macrocycles. *Inorg. Chem.* **2018**, *57*, 3475−3485. (c) Gao, W.-X.; Feng, H.-J.; Guo, B.-B.; Lu, Y.; Jin, G.-X. Coordination-directed construction of molecular links. *Chem. Rev.* **2020**, *120*, 6288−6325.

(3) (a) Ayme, J.-F.; Beves, J. E.; Campbell, C. J.; Gil-Ramírez, G.; Leigh, D. A.; Stephens, A. J. Strong and selective anion binding within the central cavity of molecular knots and links. *J. Am. Chem. Soc.* **2015**, *137*, 9812−9815. (b) Bilbeisi, R. A.; Prakasam, T.; Lusi, M.; El-

Khoury, R.; Platas-Iglesias, C.; Charbonnière, L. J.; Olsen, J.-C.; Elhabiri, M.; Trabolsi, A. [C−H···anion] interactions mediate the templation and anion binding properties of topologically non-trivial metal−organic structures in aqueous solutions. *Chem. Sci.* **2016**, *7*, 2524−253. (c) Prakasam, T.; Bilbeisi, R. A.; Lusi, M.; Olsen, J.-C.; Platas-Iglesias, C.; Trabolsi, A. Post-synthetic modifications of cadmium-based knots and links. *Chem. Commun.* **2016**, *52*, 7398−7401.

(4) (a) Marcos, V.; Stephens, A. J.; Jaramillo-Garcia, J.; Nussbaumer, A. L.; Woltering, S. L.; Valero, A.; Lemonnier, J.-F.; Vitorica-Yrezabal, I. J.; Leigh, D. A. Allosteric initiation and regulation of catalysis with a molecular knot. *Science* **2016**, *352*, 1555−1559. (b) Gil-Ramírez, G.; Hoekman, S.; Kitching, M. O.; Leigh, D. A.; Vitorica-Yrezabal, I. J.; Zhang, G. Tying a molecular overhand knot of single handedness and asymmetric catalysis with the corresponding pseudo-$D_3$-symmetric trefoil knot. *J. Am. Chem. Soc.* **2016**, *138*, 13159−13162.

(5) Tkalec, U.; Ravnik, M.; Copar, S.; Zumer, S.; Musevic, I. Reconfigurable knots and links in chiral nematic colloids. *Science* **2011**, *333*, 62−65.

(6) Benyettou, F.; Prakasam, T.; Ramdas Nair, A.; Witzel, I.-I.; Alhashimi, M.; Skorjanc, T.; Olsen, J.-C.; Sadler, K. C.; Trabolsi, A. Potent and selective *in vitro* and *in vivo* antiproliferative effects of metal−organic trefoil knots. *Chem. Sci.* **2019**, *10*, 5884−5892.

(7) Leigh, D. A.; Pirvu, L.; Schaufelberger, F.; Tetlow, D. J.; Zhang, L. Securing a supramolecular architecture by tying a stopper knot. *Angew. Chem., Int. Ed.* **2018**, *57*, 10484−10488.

(8) (a) Hasenknopf, B.; Lehn, J.-M.; Kneisel, B. O.; Baum, G.; Fenske, D. Self-assembly of a circular double helicate. *Angew. Chem., Int. Ed. Engl.* **1996**, *35*, 1838−1840. (b) Hasenknopf, B.; Lehn, J.-M.; Boumediene, N.; Dupont-Gervais, A.; Van Dorsselaer, A.; Kneisel, B.; Fenske, D. Self-assembly of tetra- and hexanuclear circular helicates. *J. Am. Chem. Soc.* **1997**, *119*, 10956−10962. (c) Hasenknopf, B.; Lehn, J.-M.; Boumediene, N.; Leize, E.; Van Dorsselaer, A. Kinetic and thermodynamic control in self-assembly: Sequential formation of linear and circular helicates. *Angew. Chem., Int. Ed.* **1998**, *37*, 3265−3268.

(9) (a) Ayme, J.-F.; Beves, J. E.; Leigh, D. A.; McBurney, R. T.; Rissanen, K.; Schultz, D. A synthetic molecular pentafoil knot. *Nat. Chem.* **2012**, *4*, 15−20. (b) Ayme, J.-F.; Beves, J. E.; Leigh, D. A.; McBurney, R. T.; Rissanen, K.; Schultz, D. Pentameric circular iron(II) double helicates and a molecular pentafoil knot. *J. Am. Chem. Soc.* **2012**, *134*, 9488−9497. (c) Leigh, D. A.; Pritchard, R. G.; Stephens, A. J. A Star of David Catenane. *Nat. Chem.* **2014**, *6*, 978−982. (d) Danon, J. J.; Krüger, A.; Leigh, D. A.; Lemonnier, J.-F.; Stephens, A. J.; Vitorica-Yrezabal, I. J.; Woltering, S. L. Braiding a molecular knot with eight crossings. *Science* **2017**, *355*, 159−162. (e) Zhang, L.; August, D. P.; Zhong, J.; Whitehead, G. F. S.; Vitorica-Yrezabal, I. J.; Leigh, D. A. A molecular trefoil knot from a trimeric circular helicate. *J. Am. Chem. Soc.* **2018**, *140*, 4982−4985. (f) Danon, J. J.; Leigh, D. A.; Pisano, S.; Valero, A.; Vitorica-Yrezabal, I. J. A six-crossing doubly interlocked [2]catenane with twisted rings, and a molecular granny knot. *Angew. Chem., Int. Ed.* **2018**, *57*, 13833−13837. (g) Zhang, L.; Stephens, A. J.; Nussbaumer, A. L.; Lemonnier, J.-F.; Jurček, P.; Vitorica-Yrezabal, I. J.; Leigh, D. A. Stereoselective synthesis of a composite knot with nine crossings. *Nat. Chem.* **2018**, *10*, 1083−1088.

(10) (a) Gale, P. A.; Davis, J. T.; Quesada, R. Anion transport and supramolecular medicinal chemistry. *Chem. Soc. Rev.* **2017**, *46*, 2497−2519. (b) Wu, X.; Howe, E. N. W.; Gale, P. A. Supramolecular transmembrane anion transport: New assays and insights. *Acc. Chem. Res.* **2018**, *51*, 1870−1879. (c) Kim, D. S.; Sessler, J. L. Calix[4]pyrroles: Versatile molecular containers with ion transport, recognition, and molecular switching functions. *Chem. Soc. Rev.* **2015**, *44*, 532−546. (d) Davis, A. P.; Sheppard, D. N.; Smith, B. D. Development of synthetic membrane transporters for anions. *Chem. Soc. Rev.* **2007**, *36*, 348−357.

(11) (a) Unwin, N. The structure of ion channels in membranes of excitable cells. *Neuron* **1989**, *3*, 665−676. (b) Hübner, C. A.; Jentsch, T. J. Ion channel diseases. *Hum. Mol. Genet.* **2002**, *11*, 2435−2445.

(12) (a) Fyles, T. M. Synthetic ion channels in bilayer membranes. *Chem. Soc. Rev.* **2007**, *36*, 335−347. (b) Reiss, P.; Koert, U. Ion-channels: Goals for function-oriented synthesis. *Acc. Chem. Res.* **2013**, *46*, 2773−2780. (c) Gokel, G. W.; Negin, S. Synthetic ion channels: From pores to biological applications. *Acc. Chem. Res.* **2013**, *46*, 2824−2833. (d) Sakai, N.; Matile, S. Synthetic ion channels. *Langmuir* **2013**, *29*, 9031−9040. (e) Si, W.; Xin, P.; Li, Z.-T.; Hou, J.-L. Tubular unimolecular transmembrane channels: Construction strategy and transport activities. *Acc. Chem. Res.* **2015**, *48*, 1612−1619. (f) Feng, W.-X.; Sun, Z.; Barboiu, M. Pillar[n]arenes for construction of artificial transmembrane channels. *Isr. J. Chem.* **2018**, *58*, 1209. (g) Chen, J.-Y.; Hou, J.-L. Controllable synthetic ion channels. *Org. Chem. Front.* **2018**, *5*, 1728−1736.

(13) (a) Ghadiri, M. R.; Granja, J. R.; Milligan, R. A.; McRee, D. E.; Khazanovich, N. Self-assembling organic nanotubes based on a cyclic peptide architecture. *Nature* **1993**, *366*, 324−327. (b) Montenegro, J.; Ghadiri, M. R.; Granja, J. R. Ion channel models based on self-assembling cyclic peptide nanotubes. *Acc. Chem. Res.* **2013**, *46*, 2955−2965. (c) Otis, F.; Auger, M.; Voyer, N. Exploiting peptide nanostructures to construct functional artificial ion channels. *Acc. Chem. Res.* **2013**, *46*, 2934−2943. (d) Jones, J. E.; Diemer, V.; Adam, C.; Raftery, J.; Ruscoe, R. E.; Sengel, J. T.; Wallace, M. I.; Bader, A.; Cockroft, S. L.; Clayden, J.; Webb, S. J. Length-dependent formation of transmembrane pores by $3_{10}$-helical $\alpha$-aminoisobutyric acid foldamers. *J. Am. Chem. Soc.* **2016**, *138*, 688−695. (e) Adam, C.; Peters, A. D.; Lizio, M. G.; Whitehead, G. F. S.; Diemer, V.; Cooper, J. A.; Cockroft, S. L.; Clayden, J.; Webb, S. J. The role of terminal functionality in the membrane and antibacterial activity of peptaibol-mimetic Aib foldamers. *Chem. - Eur. J.* **2018**, *24*, 2249−2256. (f) Tripathi, P.; Shuai, L.; Joshi, H.; Yamazaki, H.; Fowle, W. H.; Aksimentiev, A.; Fenniri, H.; Wanunu, M. Rosette nanotube porins as ion selective transporters and single-molecule sensors. *J. Am. Chem. Soc.* **2020**, *142*, 1680−1685. (g) Peters, A. D.; Borsley, S.; della Sala, F.; Cairns-Gibson, D. F.; Leonidou, M.; Clayden, J.; Whitehead, G. F. S.; Vitorica-Yrezabal, I. J.; Takano, E.; Burthem, J.; Cockroft, S. L.; Webb, S. Switchable foldamer ion channels with antibacterial activity. *Chem. Sci.* **2020**, *11*, 7023−7030.

(14) (a) Baumeister, B.; Sakai, N.; Matile, S. *p*-Octiphenyl $\beta$-barrels with ion channel and esterase activity. *Org. Lett.* **2001**, *3*, 4229−4232. (b) Bhosale, S.; Sisson, A. L.; Talukdar, P.; Fürstenberg, A.; Banerji, N.; Vauthey, E.; Bollot, G.; Mareda, J.; Röger, C.; Würthner, F.; Sakai, N.; Matile, S. Photoproduction of proton gradients with $\pi$-stacked fluorophore scaffolds in lipid bilayers. *Science* **2006**, *313*, 84−86. (c) Wei, X.; Zhang, G.; Shen, Y.; Zhong, Y.; Liu, R.; Yang, N.; Al-Mkhaizim, F. Y.; Kline, M. A.; He, L.; Li, M.; Lu, Z.-L.; Shao, Z.; Gong, B. Persistent organic nanopores amenable to structural and functional tuning. *J. Am. Chem. Soc.* **2016**, *138*, 2749−2754.

(15) (a) Benke, B. P.; Aich, P.; Kim, Y.; Kim, K. L.; Rohman, M. R.; Hong, S.; Hwang, I.-C.; Lee, E. H.; Roh, J. H.; Kim, K. Iodide-selective synthetic ion channels based on shape-persistent organic cages. *J. Am. Chem. Soc.* **2017**, *139*, 7432−7435. (b) Jung, M.; Kim, H.; Baek, K.; Kim, K. Synthetic ion channel based on metal−organic polyhedra. *Angew. Chem., Int. Ed.* **2008**, *47*, 5755−5757. (c) Haynes, C. J. E.; Zhu, J.; Chimerel, C.; Hernandez-Ainsa, S.; Riddell, I. A.; Ronson, T. K.; Keyser, U. F.; Nitschke, J. R. Blockable $Zn_{10}L_{15}$ ion channels through subcomponent self-assembly. *Angew. Chem., Int. Ed.* **2017**, *56*, 15388−15392. (d) De Riccardis, F.; Izzo, I.; Montesarchio, D.; Tecilla, P. Ion transport through lipid bilayers by synthetic ionophores: Modulation of activity and selectivity. *Acc. Chem. Res.* **2013**, *46*, 2781−2790. (e) Fyles, T. M.; Tong, C. C. Long-lived and highly conducting ion channels formed by lipophilic ethylenediamine palladium(II) complexes. *New J. Chem.* **2007**, *31*, 655−661. (f) Wilson, C. P.; Webb, S. J. Palladium(II)-gated ion channels. *Chem. Commun.* **2008**, 4007−4009. (g) Zheng, S.-P.; Huang, L.-B.; Sun, Z.; Barboiu, M. Self-assembled artificial ion-channels toward natural selection of functions. *Angew. Chem., Int. Ed.* **2020**, DOI: 10.1002/anie.201915287.



https://dx.doi.org/10.1021/jacs.0c07977
J. Am. Chem. Soc. 2020, 142, 18859−18865

(16) Kano, K.; Fendler, J. H. Pyranine as a sensitive pH probe for liposome interiors and surfaces. pH gradients across phospholipid vesicles. *Biochim. Biophys. Acta, Biomembr.* **1978**, *509*, 289−299.
(17) Di Giorgio, A. F.; Otto, S.; Bandyopadhyay, P.; Regen, S. L. Ion conductors that favor passive transport in ergosterol-rich over cholesterol-rich phospholipid membranes. *J. Am. Chem. Soc.* **2000**, *122*, 11029−11030.
(18) (a) Merritt, E. A.; Sarfaty, S.; Van den Akker, F.; L'Hoir, C.; Martial, J. A.; Hol, W. G. J. Crystal-structure of cholera-toxin B-pentamer bound to receptor $G_{M1}$ pentasaccharide. *Protein Sci.* **1994**, *3*, 166−175. (b) Zhang, R.-G.; Scott, D. L.; Westbrook, M. L.; Nance, S.; Spangler, B. D.; Shipley, G. G.; Westbrook, E. M. The three-dimensional crystal structure of cholera toxin. *J. Mol. Biol.* **1995**, *251*, 563−573. (c) Czajkowsky, D. M.; Sheng, S.; Shao, Z. Staphylococcal $\alpha$-hemolysin can form hexamers in phospholipid bilayers. *J. Mol. Biol.* **1998**, *276*, 325−330. (d) Furini, S.; Domene, C.; Rossi, M.; Tartagni, M.; Cavalcanti, S. Model-based prediction of the $\alpha$-hemolysin structure in the hexameric state. *Biophys. J.* **2008**, *95*, 2265−2274.
(19) (a) Collins, K. D.; Washabaugh, M. W. The Hofmeister effect and the behaviour of water at interfaces. *Q. Rev. Biophys.* **1985**, *18*, 323−422. (b) Kunz, W.; Lo Nostro, P.; Ninham, B. W. The present state of affairs with Hofmeister effects. *Curr. Opin. Colloid Interface Sci.* **2004**, *9*, 1−18. (c) Zhang, Y. J.; Cremer, P. S. Interactions between macromolecules and ions: The Hofmeister series. *Curr. Opin. Chem. Biol.* **2006**, *10*, 658−663. (d) Pegram, L. M.; Record, M. T. Thermodynamic origin of Hofmeister ion effects. *J. Phys. Chem. B* **2008**, *112*, 9428−9436.
(20) Marcus, Y. Thermodynamics of solvation of ions. Part 5.—Gibbs free energy of hydration at 298.15 K. *J. Chem. Soc., Faraday Trans.* **1991**, *87*, 2995−2999.
(21) Eisenman, G.; Horn, R. The role of kinetic and equilibrium processes in ion permeation through channels. *J. Membr. Biol.* **1983**, *76*, 197−225.
(22) (a) Marcus, Y. Ionic radii in aqueous solutions. *Chem. Rev.* **1988**, *88*, 1475−1498. (b) Shannon, R. D. Revised effective ionic radii and systematic studies of interatomic distances in halides and chalcogenides. *Acta Crystallogr., Sect. A: Cryst. Phys., Diffr., Theor. Gen. Crystallogr.* **1976**, *32*, 751−767.
(23) (a) Sidorov, V.; Kotch, F. W.; Abdrakhmanova, G.; Mizani, R.; Fettinger, J. C.; Davis, J. T. Ion channel formation from a calix[4]arene amide that binds HCl. *J. Am. Chem. Soc.* **2002**, *124*, 2267−2278. (b) Li, X.; Shen, B.; Yao, X.-Q.; Yang, D. A small synthetic molecule forms chloride channels to mediate chloride transport across cell membranes. *J. Am. Chem. Soc.* **2007**, *129*, 7264−7265. (c) Gorteau, V.; Bollot, G.; Mareda, J.; Perez-Velasco, A.; Matile, S. Rigid oligonaphthalenediimide rods as transmembrane anion−$\pi$ slides. *J. Am. Chem. Soc.* **2006**, *128*, 14788−14789. (d) Gorteau, V.; Bollot, G.; Mareda, J.; Matile, S. Rigid-rod anion−$\pi$ slides for multiion hopping across lipid bilayers. *Org. Biomol. Chem.* **2007**, *5*, 3000−3012. (e) Hennig, A.; Fischer, L.; Guichard, G.; Matile, S. Anion−macrodipole interactions: Self-assembling oligourea/amide macrocycles as anion transporters that respond to membrane polarization. *J. Am. Chem. Soc.* **2009**, *131*, 16889−16895. (f) Vidal, M.; Schmitzer, A. Molecular parameters and transmembrane transport mechanism of imidazolium-functionalized binols. *Chem. - Eur. J.* **2014**, *20*, 9998−10004. (g) Saha, T.; Gautam, A.; Mukherjee, A.; Lahiri, M.; Talukdar, P. Chloride transport through supramolecular barrel-rosette ion channels: Lipophilic control and apoptosis-inducing activity. *J. Am. Chem. Soc.* **2016**, *138*, 16443−16451.
(24) Pajewski, R.; Ferdani, R.; Pajewska, J.; Djedovič, N.; Schlesinger, P. H.; Gokel, G. W. Evidence for dimer formation by an amphiphilic heptapeptide that mediates chloride and carboxyfluorescein release from liposomes. *Org. Biomol. Chem.* **2005**, *3*, 619−625.
(25) Matile, S.; Sakai, N.; Hennig, A. Transport Experiments in Membranes. In *Supramolecular Chemistry: From Molecules to Nanomaterials*; Gale, P. A., Steed, J. W., Eds.; John Wiley & Sons, Ltd: Hoboken, NJ, 2012; pp 473−499.
(26) Chui, J. K. W.; Fyles, T. M. Ionic conductance of synthetic channels: analysis, lessons, and recommendations. *Chem. Soc. Rev.* **2012**, *41*, 148−175.
(27) (a) Muller, R. U.; Peskin, C. S. The kinetics of monazomycin-induced voltage-dependent conductance. I. Proof of the validity of an empirical rate equation. *J. Gen. Physiol.* **1981**, *78*, 201−229. (b) Borsley, S.; Haugland, M. M.; Oldknow, S.; Cooper, J. A.; Burke, M. J.; Scott, A.; Grantham, W.; Vallejo, J.; Brechin, E. K.; Lusby, P. J.; Cockroft, S. L. Electrostatic forces in field-perturbed equilibria: Nanopore analysis of cage complexes. *Chem.* **2019**, *5*, 1275−1292.
(28) Yifrach, O. Hill coefficient for estimating the magnitude of cooperativity in gating transitions of voltage-dependent ion channels. *Biophys. J.* **2004**, *87*, 822−830.
(29) Weiss, J. N. The Hill equation revisited: Uses and misuses. *FASEB J.* **1997**, *11*, 835−841.
(30) Leevy, W. M.; Donato, G. M.; Ferdani, R.; Goldman, W. E.; Schlesinger, P. H.; Gokel, G. W. Synthetic hydraphile channels of appropriate length kill *Escherichia coli*. *J. Am. Chem. Soc.* **2002**, *124*, 9022−9023.
(31) (a) Duclohier, H. Peptaibiotics and peptaibols: An alternative to classical antibiotics? *Chem. Biodiversity* **2007**, *4*, 1023−1026. (b) Chen, F. Y.; Lee, M. T.; Huang, H. W. Evidence for membrane thinning effect as the mechanism for peptide-induced pore formation. *Biophys. J.* **2003**, *84*, 3751−3758. (c) Bobone, S.; Gerelli, Y.; De Zotti, M.; Bocchinfuso, G.; Farrotti, A.; Orioni, B.; Sebastiani, F.; Latter, E.; Penfold, J.; Senesi, R.; Formaggio, F.; Palleschi, A.; Toniolo, C.; Fragneto, G.; Stella, L. Membrane thickness and the mechanism of action of the short peptaibol trichogin GA IV. *Biochim. Biophys. Acta, Biomembr.* **2013**, *1828*, 1013−1024.
(32) Gopfrich, K.; Li, C. Y.; Mames, I.; Bhamidimarri, S. P.; Ricci, M.; Yoo, J.; Mames, A.; Ohmann, A.; Winterhalter, M.; Stulz, E.; Aksimentiev, A.; Keyser, U. F. Ion channels made from a single membrane-spanning DNA duplex. *Nano Lett.* **2016**, *16*, 4665−4669.
(33) (a) Soto-Cerrato, V.; Manuel-Manresa, P.; Hernando, E.; Calabuig-Fariñas, S.; Martínez-Romero, A.; Fernández-Dueñas, V.; Sahlholm, K.; Knöpfel, T.; García-Valverde, M.; Rodilla, A. M.; Jantus-Lewintre, E.; Farràs, R.; Ciruela, F.; Pérez-Tomás, R.; Quesada, R. Facilitated anion transport induces hyperpolarization of the cell membrane that triggers differentiation and cell death in cancer stem cells. *J. Am. Chem. Soc.* **2015**, *137*, 15892−15898. (b) Ko, S.-K.; Kim, S. K.; Share, A.; Lynch, V. M.; Park, J.; Namkung, W.; van Rossom, W.; Busschaert, N.; Gale, P. A.; Sessler, J. L.; Shin, I. Synthetic ion transporters can induce apoptosis by facilitating chloride anion transport into cells. *Nat. Chem.* **2014**, *6*, 885−892. (c) Wu, X.; Judd, L. W.; Howe, E. N. W.; Withecombe, A. M.; Soto-Cerrato, V.; Li, H.; Busschaert, N.; Valkenier, H.; Pérez-Tomas, R.; Sheppard, D. N.; Jiang, Y.-B.; Davis, A. P.; Gale, P. A. Nonprotonophoric electrogenic $Cl^-$ transport mediated by valinomycin-like carriers. *Chem.* **2016**, *1*, 127−146.
(34) Stoddart, J. F. Dawning of the age of molecular nanotopology. *Nano Lett.* **2020**, *20*, 5597−5600.
(35) Zhang, L.; Stephens, A. J.; Lemonnier, J.-F.; Pirvu, L.; Vitorica-Yrezabal, I. J.; Robinson, C. J.; Leigh, D. A. Coordination chemistry of a molecular pentafoil knot. *J. Am. Chem. Soc.* **2019**, *141*, 3952−3958.


https://dx.doi.org/10.1021/jacs.0c07977
J. Am. Chem. Soc. 2020, 142, 18859−18865